

Prediction of inelastic response periods of buildings based on intensity measures and analytical model parameters

E.I. Katsanos ^a, A.G. Sextos ^{a,*}, A.S. Elnashai ^b

^a Department of Civil Engineering, Aristotle University, Thessaloniki 54124, Greece

^b Department of Civil and Environmental Engineering, University of Illinois, Urbana, IL 61801, USA



ARTICLE INFO

Article history:

Received 22 September 2013

Revised 7 March 2014

Accepted 4 April 2014

Available online 3 May 2014

Keywords:

RC buildings

Period elongation

Inelastic response

Degrading hysteretic rules

Response history analysis

ABSTRACT

This paper investigates the elongation of the fundamental period of reinforced concrete buildings that occurs during earthquake loading and its correlation with various intensity measures and engineering demand parameters. For this purpose, five buildings designed according to modern seismic codes are studied through equivalent single degree of freedom nonlinear systems with hysteretic laws that represent various levels of stiffness degradation, strength deterioration and pinching. By means of an extensive parametric analysis using a large set of earthquake ground motions and a rigorous validation procedure, the period elongation is quantitatively assessed as a function of building configuration and design (structural system and ductility class), ground motion characteristics (peak ground acceleration, spectral acceleration, frequency content) and demand parameters (displacement ductility). The results indicate that structures, designed according to modern seismic codes, are expected to exhibit low-to-moderate period elongation even for twice the intensity of the design earthquake. Given that the fundamental period of buildings is a key parameter in most seismic code procedures for ground motion selection, design and assessment, the implications of the predicted period lengthening are also discussed. The results are of interest to designers and analysts, as well as code-development committees.

© 2014 Elsevier Ltd. All rights reserved.

1. Introduction

During earthquake ground shaking, reinforced concrete (R/C) buildings experience deterioration in strength and stiffness because of concrete cracking and crushing, as well as yielding of the reinforcing bars of the structural members. The ability of these members to dissipate seismic energy is also reduced with the number of load reversals. Therefore, it has been long recognized that after the first significant excursion beyond the yield limit, the structures begin to soften and respond with gradually higher apparent natural periods [1].

The elongated fundamental period, as an implicit indicator of the degree of inelasticity that structures exhibit under earthquake loading, is a key parameter to establish a rigorous evaluation of the structural performance into the nonlinear regime and as such, it has long attracted scientific attention. One of the first fundamental observations was that, the earthquake-imposed structural damage (i.e., inelastic response) and the modification of the dynamic characteristics of structures (i.e., vibration modes and periods) are closely correlated [2]. Identifying the physical significance of

the predominant (maximum) inelastic period considered as an implicit indicator of the inelastic structural response, various damage models based on period lengthening have been proposed to evaluate the global structural damage of R/C buildings (i.e., [3–5]). Furthermore, a spectrum ground motion intensity measure (IM), explicitly accounting for period lengthening, improved the correlation between ground motion and nonlinear response, compared with the use of conventional IMs [6].

The time-variant natural frequency of structures has been investigated either by the measured seismic response of instrumented buildings [7–11], or by experimentally studying the period shift attributed to successive inelastic episodes in full-scale structural models [12–15]. Still though, the amplitude of period elongation is a contradictory issue within the earthquake engineering community. In fact, several researchers [8,16] have observed that the vibration period of R/C buildings may be strongly elongated during strong ground shaking (up to 100–130%), while only moderate lengthening of the fundamental period (up to 50–70%) has been observed by others [17,18]. Notwithstanding the advances already made, most research results are case-specific, while the number of structural systems studied and seismic motions used is limited.

* Corresponding author.

E-mail addresses: asextos@civil.auth.gr, asextos@gmail.com (A.G. Sextos).

Another significant implication of earthquake induced-period lengthening is that the latter is a key parameter in the ground motion selection and scaling procedure, as most current seismic codes define the spectral matching period bandwidth on the basis of the fundamental period of structures. This is of particular interest for Eurocode 8 [19], which, in contrast to the US codes and guidelines such as ASCE/SEI 7-10 [20] and FEMA P-750 [21], enforces a wider spectral matching period range that extends up to twice the fundamental period of the building (as opposed to 1.5 times prescribed in the US). This difference may potentially result in overconservative and highly scattered estimates of seismic demand for reasons described elsewhere [22].

To investigate further the extent of period elongation during strong ground motion and its implications in the design and assessment of structures, a group of five R/C buildings [23] with various structural configurations and dynamic characteristics was thoroughly studied. The buildings, designed deliberately for various ductility classes according to modern seismic codes (herein Eurocode 8), were transformed into equivalent nonlinear single-degree-of-freedom (SDOF) systems [24] of various hysteretic rules and then they were subjected to a set of carefully selected ground motions. In the following, the correlation patterns observed between the numerically predicted periods lengthening of the five buildings studied, the structural properties and the ground motion characteristics are presented and critically assessed.

2. Strong ground motion selection

In contrast to the common practice where ground motion selection is either based on a given, site-specific seismic hazard scenario, or involves a small number of recorded ground motions (which typically does not exceed seven), the scope of the particular investigation dictated the formation of a large ensemble of earthquake records with a wealth of different characteristics. For this purpose, an ensemble of 300 seismic motions was formed according to particular selection rules to prevent undesirable bias. More precisely:

- (a) Forty-three (43) different earthquake events recorded in various regions worldwide were employed to avoid dominating the ensemble with records from areas with common seismotectonic features.
- (b) The maximum number of records from the same earthquake event was limited to less than 15% of the total, while only one of the two horizontal components was used from the same station.
- (c) The preliminary selection criteria related to seismological characteristics (i.e., magnitude, rupture mechanism, directivity of seismic waves), amplitude (peak ground acceleration) and soil profile were deliberately kept wide.
- (d) Both near-and far-field seismic motions were used to provide high amplifications in a wide range of structural periods. Given that the aim of the study is to investigate

the predominant inelastic period under strong ground motion, short duration motions were filtered-out (i.e., a $M_w > 5.5$ criterion was adopted), as weaker motions would statistically lead to lower ductility demand. Fig. 1 illustrates the distribution of the selected strong motion characteristics in terms of earthquake magnitude, source-to-site distance, peak ground acceleration (PGA) and mean period.

- (e) The mean period parameter (T_m) was introduced, to quantify the predominant frequency content of the records used [25], as a means to retain the ensemble as uniformly distributed as possible. Different intervals of T_m , indicative of high, moderate and low-frequency content, were defined (Table 1) and three frequency-based subsets of 100 records were formed, each characterized by high spectral amplifications in the short, moderate and long period range respectively. It is recalled that the mean period, T_m , is derived by weighting the amplitudes over a specified range of the Fourier Amplitude Spectrum (FAS):

$$T_m = \frac{\sum C_i^2 f_i}{\sum C_i^2} \quad \text{for } 0.25 \text{ Hz} \leq f_i \leq 20 \text{ Hz} \text{ with } \Delta f \leq 0.05 \text{ Hz} \quad (1)$$

where C_i are the Fourier amplitude coefficients, f_i are the discrete Fast Fourier Transformation (FFT) frequencies between 0.25 and 20 Hz and Δf is the frequency interval used in the FFT.

Based on the above criteria, the ground motions summarized in Table 2 were retrieved by the PEER-NGA Database [26] and were later applied for the excitation of the five R/C buildings presented in the following section.

3. Structural models

3.1. Multiple degree of freedom systems

The structures selected for this investigation have been extensively studied in the past [23,27,28] and represent alternative and realistic structural configurations in terms of the earthquake resistant system (frame or dual), their ductility level (Classes High and Low according to the Eurocode 8) and their overall height (and subsequently, their fundamental period). Live loads and permanent gravity load are both assumed equal to 2.0 kN/m². All buildings are assumed to be supported on (firm) soil class 'B' according to EC8. The characteristic cylinder strength of concrete was taken 30 N/mm² and the yield strength of steel equal to 585 N/mm² for both longitudinal and transverse reinforcement. More details regarding member cross section sizes and reinforcements are given in [27].

It is noted that the intention was to examine buildings designed to modern seismic codes in order to focus on a better-controlled stock with identical level of seismic safety. On the other hand, it is evident that existing, pre-code, or under-designed structures

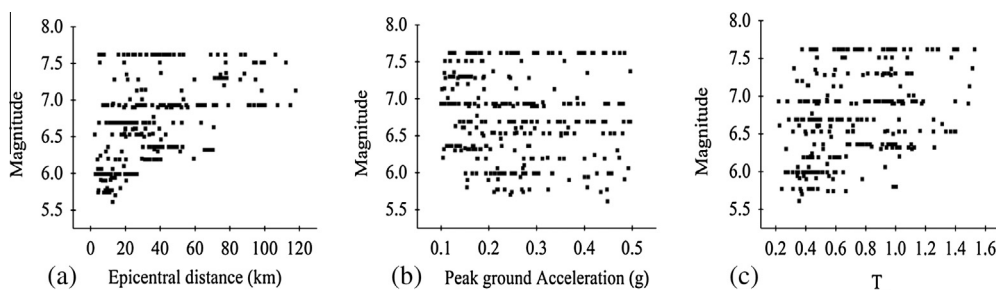


Fig. 1. Distribution of the selected strong motion characteristics in terms of earthquake magnitude, source-to-site distance, peak ground acceleration and mean period.

Table 1Distribution of selected earthquake ground motions in terms of their mean period T_m .

Subset number	T_m interval (s)	Number of records	25th Percentile (Q1) of T_m (s)	50th Percentile (Q2) of T_m (s)	75th Percentile (Q3) of T_m (s)
1	0.10–0.50	100	0.30	0.37	0.44
2	0.50–0.90	100	0.58	0.66	0.78
3	0.90–1.55	100	0.99	1.08	1.19

Table 2

Earthquake events used in the study and related information (retrieved from PEER-NGA Database, Chiou et al. [26]).

Earthquake name (date)	Magnitude, M_w	Number of records	Distance (km) R_{min} – R_{max}	Site class ^{a,b}
Kern County (1952.07.21)	7.36	1	88.39	C(1)
North. California (1954.12.21)	6.50	1	30.79	D(1)
Parkfield (1966.06.28)	6.19	3	32.56–40.26	C(1) + D(2)
Borrego Mountain (1968.04.09)	6.63	1	70.75	D(1)
San Fernando (1971.02.09)	6.61	5	20.04–39.49	C(4) + D(1)
Managua, Nicaragua (1972.12.23)	6.24	1	5.68	D(1)
Friuli, Italy (1976.05.06)	6.50	1	20.23	C(1)
Tabas, Iran (1978.09.16)	7.35	2	20.63–74.66	C(1) + D(1)
Coyote Lake (1979.08.06)	5.74	4	4.37–10.94	C(1) + D(3)
Imperial Valley (1979.10.15)	6.53	18	2.47–43.15	D(18)
Livermore (1980.01.24)	5.80	1	17.13	D(1)
Mammoth Lakes (1980.05.25)	5.94	7	5.90–14.19	D(7)
Victoria, Mexico (1980.06.09)	6.33	1	36.67	D(1)
Trinidad and Tobago (1980.11.08)	7.20	2	76.75	D(2)
Corinth, Greece (1981.02.24)	6.60	1	19.92	D(1)
Westmorland (1981.04.26)	5.90	3	7.02–20.47	D(3)
Coalinga (1983.05.02)	6.36	22	4.60–52.86	C(9) + D(13)
Morgan Hill (1984.04.24)	6.19	5	3.94–38.20	C(2) + D(3)
Taiwan-SMART1-40 (1986.05.20)	6.32	8	65.48–70.27	D(8)
N.Palm Springs (1986.07.08)	6.06	2	4.24–6.28	D(2)
Chalfant Valley (1986.07.20)	6.19	4	10.54–31.25	D(4)
San Salvador, El Salv. (1986.10.10)	5.80	1	9.54	D(1)
Taiwan-SMART1-45 (1986.11.14)	7.30	15	71.35–78.21	C(1) + D(14)
New Zealand (1987.03.02)	6.60	1	24.23	C(1)
Whittier Narrows (1987.10.01)	5.99	25	2.86–26.55	C(11) + D(14)
Superstition Hills (1987.11.24)	6.54	3	19.51–35.83	D(3)
Spitak, Armenia (1988.12.07)	6.77	1	36.19	D(1)
Loma Prieta (1989.10.18)	6.93	42	7.17–114.87	B(1) + C(19) + D(17) + E(5)
Manjil, Iran (1990.06.20)	7.37	2	40.43–77.84	C(1) + D(1)
Sierra Madre (1991.06.28)	5.61	1	12.64	C(1)
Erzincan, Turkey (1992.03.13)	6.69	1	8.97	D(1)
Cape Mendocino (1992.04.25)	7.01	3	22.64–53.34	C(1) + D(2)
Landers (1992.06.28)	7.28	6	13.67–94.77	C(2) + D(4)
Big Bear (1992.06.28)	6.46	1	40.46	D(1)
Northridge (1994.01.17)	6.69	33	4.85–63.53	A(1) + B(1) + C(16) + D(15)
Kobe, Japan (1995.01.16)	6.90	10	19.25–55.81	A(1) + D(9)
Northwest China (1997.04.11)	6.10	1	19.11	D(1)
Kocaeli, Turkey (1999.08.17)	7.51	9	5.31–112.26	B(1) + C(1) + D(6) + E(1)
Chi-Chi, Taiwan-1 (1999.09.20)	7.62	39	4.96–106.20	C(31) + D(8)
Chi-Chi, Taiwan-2 (1999.09.20)	6.20	3	10.10–59.29	C(2) + D(1)
Chi-Chi, Taiwan-3 (1999.09.25)	6.30	4	8.80–51.51	C(2) + D(2)
Hector Mine (1999.10.16)	7.13	4	26.53–117.88	C(2) + D(2)
Duzce, Turkey (1999.11.12)	7.14	2	29.27–31.56	C(1) + D(1)

^a According to the NEHRP site classification: Site class A ($v_{s,30} \geq 1500$ m/s), Site class B ($760 \text{ m/s} < v_{s,30} \leq 1500 \text{ m/s}$), Site class C ($360 \text{ m/s} < v_{s,30} \leq 760 \text{ m/s}$), Site class D ($180 \text{ m/s} < v_{s,30} \leq 360 \text{ m/s}$) and Site class E ($v_{s,30} \leq 180$).

^b In the last column, number in the parenthesis indicates the number of records for given site class.

with low yield strength are expected to be more prone to inelastic deformations and thus, to period lengthening or vulnerable to premature failure due to inadequate shear strength. For this reason, the results of this study, strictly speaking, only apply to buildings designed to modern seismic codes.

The five buildings studied herein are illustrated in Fig. 2 and can be classified into three principal categories: regular 12-storey frames of low and high ductility (codified as 12RFDC1 and 12RFDC1H respectively), regular 8-storey dual systems again of low and high ductility (8SWDCL and 8SWDCH) and irregular in elevation, 8-storey frame of high ductility (8IFDCH). Particularly for the latter category, irregularity in elevation refers to the greater height and the smaller amount of columns at the base storey.

All structures examined were first modeled as two-dimensional MDOF systems using the computer code Zeus-NL [29]. Cubic 3D elastoplastic elements were used to consider the concrete behavior under cyclic loading, residual strength and stiffness degradation through a fiber approach. The non-linear model used for the concrete material is a uniaxial constant confinement concrete model (Fig. 3a), defined with the use of four parameters: compressive strength, f_c , tensile strength, f_t , crushing strain, e_{co} , and the confinement factor, k [29]. Furthermore, the reinforcement bars were modeled using a bi-linear elasto-plastic law with kinematic strain hardening, provided by Zeus-NL materials library [29]. Parameters such as the Young's modulus, E , the yield strength, f_y , and the strain-hardening parameter, n , are necessary to define this model. From the eigenvalue analysis of the five building models, the

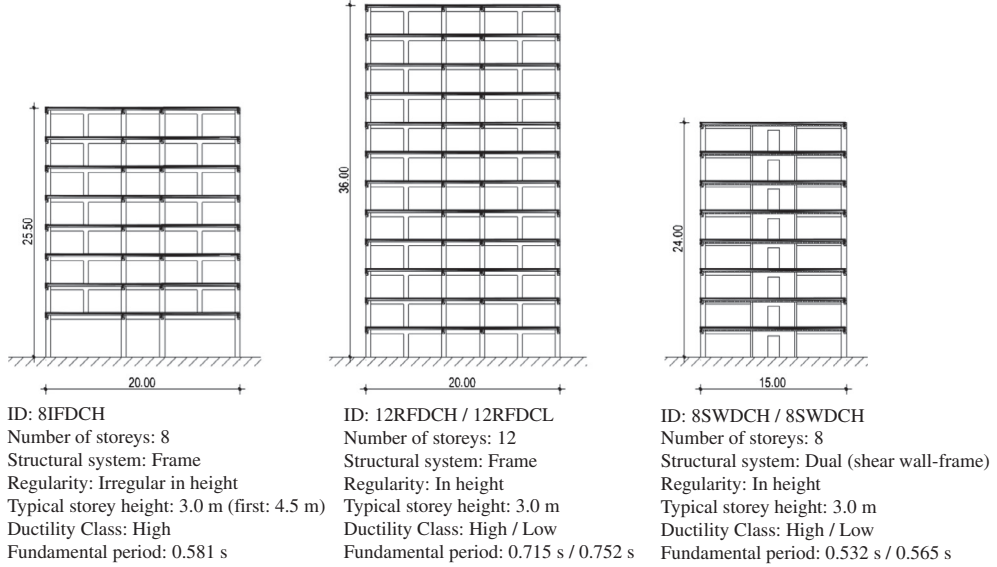


Fig. 2. Configuration of the structures examined.

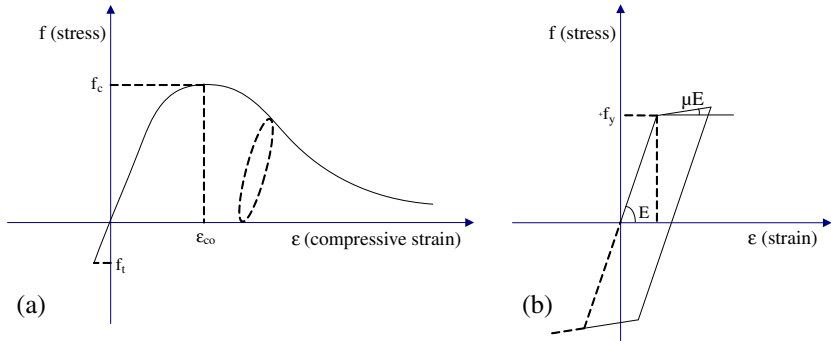


Fig. 3. (a) Non-linear uniaxial constant confinement concrete model and (b) the bilinear elasto-plastic model with kinematic strain hardening used for the steel reinforcement bars (right) [29].

elastic fundamental periods were determined as follows: 12RFDCH: $T_{el,MDOF} = 0.715$ s, 12RFDCL: $T_{el,MDOF} = 0.752$ s, 8SWDCH: $T_{el,MDOF} = 0.532$ s, 8SWDCL: $T_{el,MDOF} = 0.565$ s and 8IFDCH: $T_{el,MDOF} = 0.581$ s.

3.2. Equivalent nonlinear single degree of freedom systems

Given that extensive parametric analyses were foreseen for the five buildings using the ensemble of 300 ground motions scaled to various levels of intensity, it was considered computationally more efficient to transform the multiple degree of freedom (MDOF) systems into equivalent, nonlinear, single degree of freedom (SDOF) ones. Clearly, the transformation procedure should ensure that the (elastic and inelastic) vibration period of the latter will closely match the fundamental period of the corresponding original MDOF structures.

Along these lines, a transparent formulation, based on the N2 method [24,30], was utilized. After defining analytically the properties of the simplified nonlinear systems (namely, height, mass, deflection shape, force-displacement relationship at yield and ultimate deformation, transformation constant), the five substitute SDOF systems were modeled in IDARC-2D [31] with bilinear backbone curves (Fig. 4a) that mimic the idealized curves resulted from the Standard Pushover (SPO) analysis of the corresponding, previously derived, MDOF systems [23].

The spread plasticity element, provided by IDARC-2D, was used to model the oscillators examined, while the fiber model approach enabled the efficient capture of the inelastic response. The embedded yield-oriented model (Fig. 4b) was used to account for stiffness degradation, strength deterioration, non-symmetric response and pinching effect. A low mass-proportional damping value of 1% was also adopted. This equivalent viscous damping represents the non-hysteretic dissipation, because hysteretic damping is already considered. For validation purposes, sensitivity analyses were undertaken until it was verified that further tuning of damping was unnecessary.

The effective stiffness required for constitutive bilinear law of the SDOF system was determined by the yield point of the bilinear SPO of the MDOF system. In other words, the first (elastic) branch of the SDOF bilinear laws represent the effective (and not the purely elastic) stiffness of the corresponding MDOF systems. Thus, the elastic period of the SDOF systems was calculated equal to the effective period of the corresponding MDOF systems.

$$T_{el,SDOF} = 2\pi \sqrt{\frac{md_y}{F_y}} = T_{eff,MDOF} \quad (2)$$

where F_y , d_y and m are the yield strength, yield displacement and mass of the SDOF system respectively. The resulting elastic periods of the equivalent SDOF oscillators were found equal to 0.966 s,

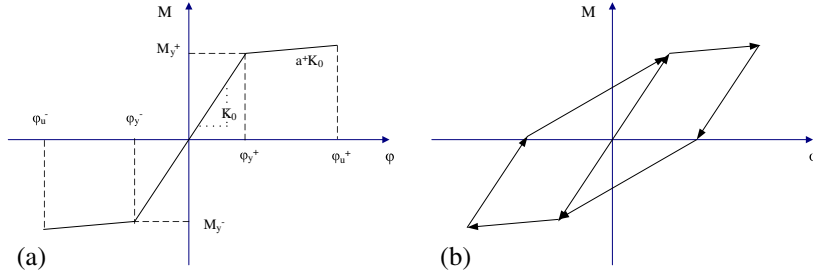


Fig. 4. (a) Bilinear backbone curve and (b) the assigned yield-oriented law for cyclic behavior (right) prescribed by the IDARC2D polygonal hysteretic model [31].

1.038 s, 0.707 s, 0.723 s and 0.804 s for the 12RFDCH, 12RFDCL, 8SWDCH, 8SWDCL, and 8IFDCH buildings, respectively.

It is recalled that the vibration periods of the SDOF systems, $T_{el,SDOF}$, have been calculated longer than the fundamental, elastic periods of the corresponding MDOF systems, $T_{el,MDOF}$ (by approximately 28–38%). This is expected given that the dynamic characteristics of the MDOF systems have been derived by eigenvalue analysis using the purely *elastic* and not *effective* properties. On the contrary, the elastic stiffness of the simplified systems is calculated identical to the effective one of the MDOF building models, since the SDOF system constitutive law mimics the idealized (bi-linear) SPO curve of the MDOF systems. That is to say, the elastic periods of the SDOF systems are essentially the effective periods of the MDOF models (Eq. (2)) and hence, $T_{el,SDOF} > T_{el,MDOF}$.

For the degrading hysteresis model adopted, four parameters control the inelastic loading reversals: α accounting for stiffness degradation, β_1 and β_2 affecting strength deterioration and the slip parameter γ that controls the pinching due to the closing of the cracks and bond slip that occurs during the reloading phase. The stiffness degradation, which occurs principally because of geometric effects and degrades with increasing ductility, was modeled using the pivot rule (Fig. 5a), developed by [32]. The stiffness degradation factor is given by:

$$R_k = \frac{M_{cur.} + aM_y}{K_0\varphi_{cur.} + aM_y} \quad (3)$$

where $M_{cur.}$ and $\varphi_{cur.}$ are the current moment and curvature developed at the section, K_0 is the initial elastic stiffness, α is the stiffness degradation parameter and M_y is the yield moment. The current (degraded) stiffness is calculated as follows:

$$K_{cur.} = R_k K_0 \quad (4)$$

Furthermore, strength deterioration is modeled by reducing the capacity in the backbone curve (Fig. 5b) according to the following rule:

$$M_{y,cur.} = M_{y,0} \left[1 - \left(\frac{\varphi_{max}}{\varphi_{ult.}} \right)^{\frac{1}{\beta_1}} \right] \left[1 - \frac{\beta_2}{1 - \beta_1} \frac{H}{H_{ult.}} \right] \quad (5)$$

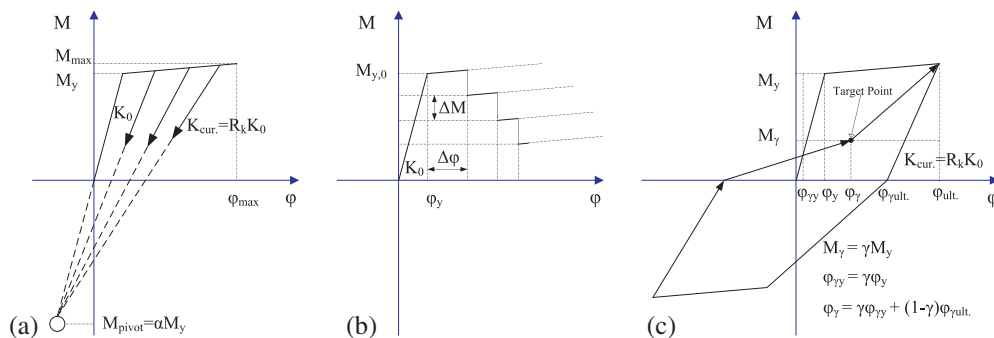


Fig. 5. Schematic representation of (a) stiffness degradation, (b) strength deterioration and (c) pinching as modeled in the IDARC-2D polygonal hysteretic model [31].

where $M_{y,cur.}$ and $M_{y,0}$ are the current (deteriorated) and initial yield moment respectively, φ_{max} and $\varphi_{ult.}$ are the maximum attained and the ultimate curvature of the section, respectively. Parameter H is the hysteretic dissipated energy and $H_{ult.}$ is the hysteretic energy dissipated when loaded monotonically to the ultimate curvature without degradation, while β_1 and β_2 are the ductility-based and energy-based strength deterioration parameters in Eq. (5). Finally, pinching is modeled by defining the target point for the loading branch to be the crack closing point. In this case, the force level (F_γ) that corresponds to this point is a fraction of the yield moment:

$$F_\gamma = \gamma F_y \quad (6)$$

The deformation level is obtained as a weighted average of the yield and ultimate deformations, as shown schematically in Fig. 5c. In this study, setting appropriate values for the degrading parameters, two degradation levels (mild and severe) were considered to envelop the period shift prediction due to the earthquake ground motion. Fig. 6 shows the effect of the degradation levels adopted on the moment-curvature relationship derived at the base of the 12RFDCH-SDOF when subjected to the Emeryville strong motion record.

4. Validation of the MDOF to the SDOF transformation

Despite the apparent benefits of using the SDOF systems instead of the MDOF ones in terms of simplicity, robustness as well as computational and time efficiency that allow for extensive, multi-parametric analyses, several limitations also exist regarding the MDOF-to-SDOF transformation procedure. One of these is related to the inability of SDOF systems to account for higher mode effects, which is particularly important for high-rise buildings or asymmetric structures with stiffness or mass irregularities in elevation and/or plan. However, the scope of this study is to investigate the correlation of the inelastic period with several ground motion characteristics and for this reason, the use of a large number of motions eliminated significantly the bias in the estimated inelastic periods that might be emerged due to the use of the SDOF systems instead of the MDOF ones. Next in this chapter, the

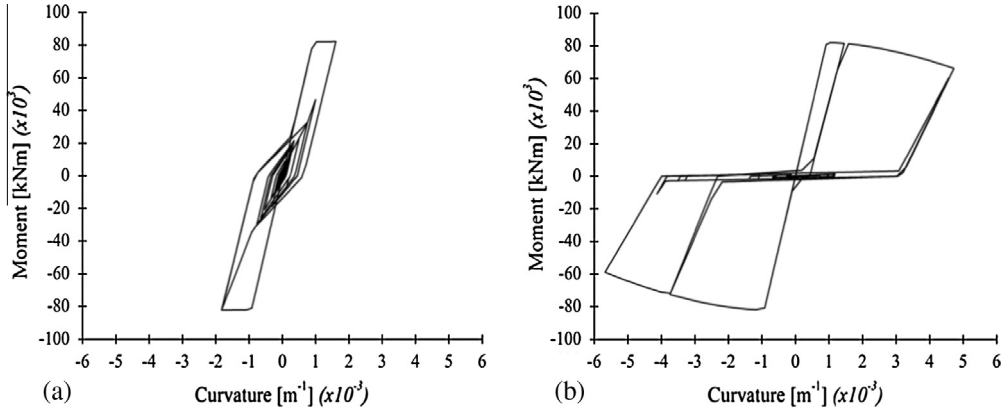


Fig. 6. Moment–curvature relationship of the 12RFDCH-SDOF system when subjected to the Emeryville record (scaled to a PGA of 0.90 g) for the case of (a) mild and (b) severe degradation rule.

reliability and accuracy of the particular MDOF–SDOF transformation procedure, in terms of the predicted periods, is clearly seen.

4.1. Elastic and inelastic stiffness

A first verification was to ensure that, indeed, the elastic and post-yield stiffness of the MDOF and SDOF systems are identical. For this purpose, a single-record incremental dynamic analysis (IDA) was performed [28,33] for all the SDOF systems considered. Fig. 7 shows the dynamic push-over curves of the equivalent SDOF systems for the 12RFDCL and 8IFDCH buildings respectively, compared to the idealized Standard Pushover curve (SPO) of the initial MDOF systems. The exact matching between these two lines verifies that the transition from the bilinear (force–displacement) SPO curve of the MDOF system, to the Moment–Curvature relationship required for the equivalent SDOF system was accurate. The same observation was reached for all other buildings and for all alternative seismic motions used.

The adoption of a tri-linear backbone curve was also examined for the equivalent SDOF systems in order to model more accurately the SPO curve of the MDOF systems. The first branch of this tri-linear law was set to capture the very initial, purely elastic stiffness of the MDOF systems (as observed in the SPO curves of the buildings studied) and thus, the equivalent SDOF systems studied had identical *elastic* period (after the eigenvalue analysis) with the MDOF ones. However, sensitivity analyses showed that this purely elastic stiffness (and hence elastic period) was very easily exceeded even for minor seismic intensity. Therefore, this approach (i.e., tri-linear law) did not provide any further accuracy for the elongated period

prediction and the inelastic period predicted was not noticeably affected by using a tri-linear moment–curvature relationship instead of using a bi-linear one.

4.2. Prediction of the mean elongated period for an ensemble of ground motions

Since the purpose of this research is to identify the correlation patterns between ground motion, structural characteristics and the elongation of the natural period of buildings designed according to modern seismic codes, it was necessary to ensure that the equivalent SDOF representations of the five buildings defined above, will eventually lead to a predominant inelastic period, which will closely match the inelastic period predicted by the reference MDOF models. It is important to note, that as the MDOF structural systems have been modeled in Zeus-NL, they account explicitly (at least in the version used to produce these results) only for stiffness degradation, while there is also a minor effect of the pinching load on the closure of the open cracks. As a result, the elongation of the fundamental period of vibration of the MDOF systems is primarily attributed to the spread of cracks and the section yielding. On the other hand, the equivalent SDOF systems, studied in IDARC-2D, do account explicitly for stiffness degradation, strength degradation and pinching but at the same time they neglect the inelastic response at a member level. For this reason, the predictions about the period elongation of the SDOF systems for this validation procedure were based on the assumption of a mild (on average) degradation rule.

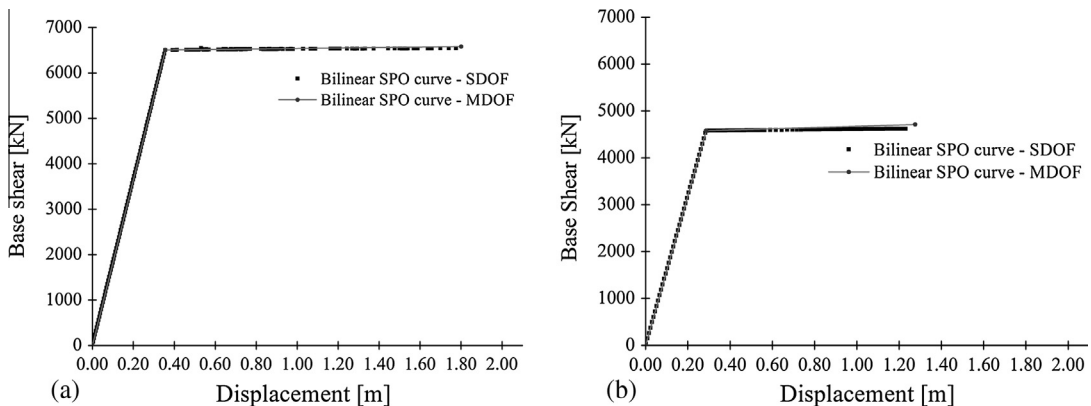


Fig. 7. Comparison between the bilinear MDOF-SPO curve and the SDOF-IDA curve for (a) the 12RFDCH and (b) the 8IFDCH buildings using the Emeryville strong motion record (Loma Prieta, 1989).

For the particular validation purpose, a subset of 20 records of the motions listed in [Table 2](#) was used, involving 15 out of the initial 43 seismic events. These records are listed in [Table 3](#) and vary in frequency content, amplitude, soil profile, and near/far-field conditions. Each record was scaled 10 times within the range 0.15–1.50 g to ensure that all models will undergo the same stages of seismic behavior: elastic response, first cracking, post-yield and severe damage. Eventually, a set of 4000 response history analyses (RHA) was performed (5 pairs of MDOF and equivalent SDOF systems, 20 ground motions, 10 scaling factors).

In all cases, the predominant inelastic period was identified through the Fast Fourier Transformation of the relative acceleration of the building top, with respect to the base acceleration. An example of this approach is illustrated in [Fig. 8](#) where the evolution of the natural frequency of vibration with increasing PGA is shown for the equivalent SDOF system of the 12RFDC building excited by the Northridge and Imperial Valley ground motions. The predominant inelastic period could be also identified accounting for a free vibration after the end of each excitation motion considered (i.e., with the use of a string of zero acceleration values for a time stretch after the end of the earthquake record in order to generate free vibration conditions). However, this technique, adopted by some researchers [[34](#)], was found to lead to lower estimates of predominant inelastic periods due to the minor influence of pinching associated with the constitutive law for (post-excitation) low intensity vibrations. It is noted that detailed comparisons, made in the frequency-time domain by means of the Wavelet Transformation, confirmed the estimates of the Fourier Spectra-based inelastic period considered herein for the entire time series, as the latter inherently include the wider stiffness degradation and pinching that takes place under strong ground motion.

[Fig. 9](#) illustrates indicatively, the period elongation prediction for the 12RFDC and 8IFDC buildings and various intensity levels (peak ground acceleration, PGA) of the Whittier Narrows and Hector Mine ground motions, that is, motions that correspond to low and high-frequency content, respectively. Firstly, it is interesting to note that even for the lowest intensity level considered (i.e., 0.15 g), the initial cracking was already occurred and hence the predominant period of the MDOF systems was calculated longer than its elastic period and identical to the elastic period of the corresponding SDOF system (e.g., for the 12RFDC model: $T_{el,MDOF} = 0.715$ s and $T_{el,SDOF} = T_{eff,MDOF} = 0.966$ s). Moreover, a reasonably good agreement is observed, at least qualitatively, even for high levels of ground motion intensity and severe associated

inelastic response, while this reasonable matching, though not presented herein, is also evident for all buildings studied and for all earthquake records used. This agreement between the MDOF and SDOF predictions is significantly improved when the comparison is made on the basis of the mean period elongation predicted for the entire ensemble of seismic records ([Figs. 10–12](#)). In this case, the bias factor (bf) between the mean inelastic period T_i^{MDOF} and T_i^{SDOF} of the MDOF and the SDOF systems respectively, for 10 levels of ground motion intensity (in terms of PGA), is given by the following expression:

$$bf = \sqrt{\frac{1}{N} \sum \left(\frac{T_i^{MDOF} - T_i^{SDOF}}{T_i^{MDOF}} \right)^2},$$

$i = 1$ to 10 levels of strong motion intensity (7)

As it is shown in [Fig. 12b](#), the bias factor between the mean inelastic period predicted by the MDOF and the SDOF systems along the range $0.15 \text{ g} < \text{PGA} < 1.50 \text{ g}$ drops to less than 10% when all the (20) records of the subset of strong motions are used. This is observed irrespectively of the building examined and despite the compromising modeling assumptions inevitably made when transforming the MDOF systems modeled in Zeus-NL to equivalent, mildly degrading SDOF systems modeled in IDARC-2D.

4.3. Sensitivity on the hysteretic rules adopted and identical triggering of inelastic response

Having obtained a level of confidence on the MDOF-to-SDOF transformation process, the parametric response history analysis (RHA) of the five equivalent SDOF systems was extended for the case of the severe degradation hysteretic rule as a means to provide an upper bound (conservative estimate) of the potential period shift due to the inelastic response. [Fig. 13](#) illustrates comparatively the period elongation as a function of ground motion intensity, for the 12RFDC building, when modeled with both mild and severe degradation rules and subjected to the Northridge and the Coyote Lake earthquake motions (i.e., motions corresponding to high and low-frequency content respectively).

It is observed that period elongation estimates from the mildly degrading model are, naturally, always lower than the ones derived when the severe degradation rule is adopted. It is also interesting to note that the inelastic response is triggered, as expected, at the same level of PGA (namely, 0.3 g for both the two seismic

Table 3
Seismic records subset used in the validation scheme.

Seismic event (date)	Recording station	Magnitude	Distance (km)	Site class	PGA (g)
Kern County (1952.07.21)	Taft Lincoln School	7.36	88.39	C	0.173
Managua, Nicaragua (1972.12.23)	Managua, ESSO	6.24	5.68	D	0.337
Coyote Lake (1979.08.06)	Gilroy Array #6	5.74	4.37	C	0.440
Imperial Valley (1979.10.15)	Delta	6.53	33.73	D	0.285
Imperial Valley (1979.10.15)	El Centro Array #10	6.53	26.31	D	0.224
Victoria, Mexico (1980.06.09)	Cerro Prietto	6.33	36.67	D	0.621
Westmorland (1981.04.26)	Westmorland Fire Station	5.90	7.02	D	0.496
Coalinga (1983.05.02)	Parkfield-Fault Zone #14	6.36	38.54	D	0.274
San Salvador, El Salv. (1986.10.10)	National Geographical Inst.	5.80	9.54	D	0.612
Whittier Narrows (1987.10.01)	Castaic-Old Ridge Route	5.99	19.81	D	0.332
Loma Prieta (1989.10.18)	Emeryville	6.93	45.50	D	0.256
Cape Mendocino (1992.04.25)	Petrolia	7.01	22.64	C	0.662
Northridge (1994.01.17)	Jensen Filter Plant	6.69	10.20	C	0.592
Northridge (1994.01.17)	Castaic-Old Bridge Route	6.69	40.68	C	0.520
Northridge (1994.01.17)	Santa Monica City Hall	6.69	22.50	D	0.369
Kobe, Japan (1995.01.16)	Amagasaki	6.90	38.79	D	0.364
Kobe, Japan (1995.01.16)	Kobe University	6.90	25.40	D	0.290
Kobe, Japan (1995.01.16)	Takatori	6.90	13.12	D	0.616
Chi-Chi, Taiwan-2 (1999.09.20)	CHY080	6.20	29.48	C	0.473
Hector Mine (1999.10.16)	Hector	7.13	26.53	C	0.266

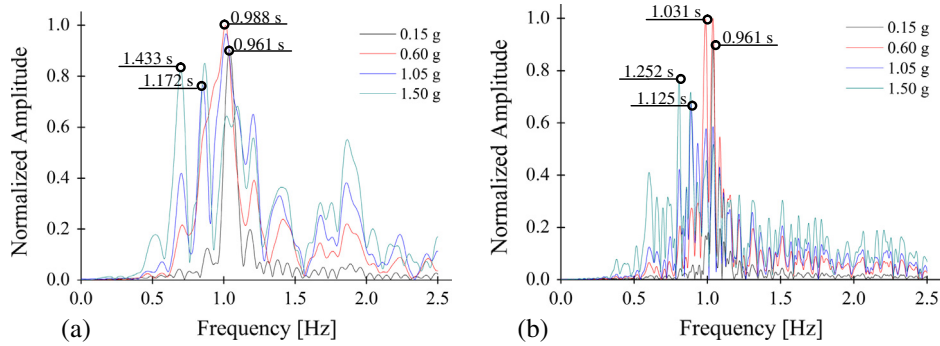


Fig. 8. Evolution of the Fourier spectrum for the 12RFDCH-SDOF equivalent system when subjected to increasing levels of (a) the Northridge and (b) Imperial Valley earthquake ground motions.

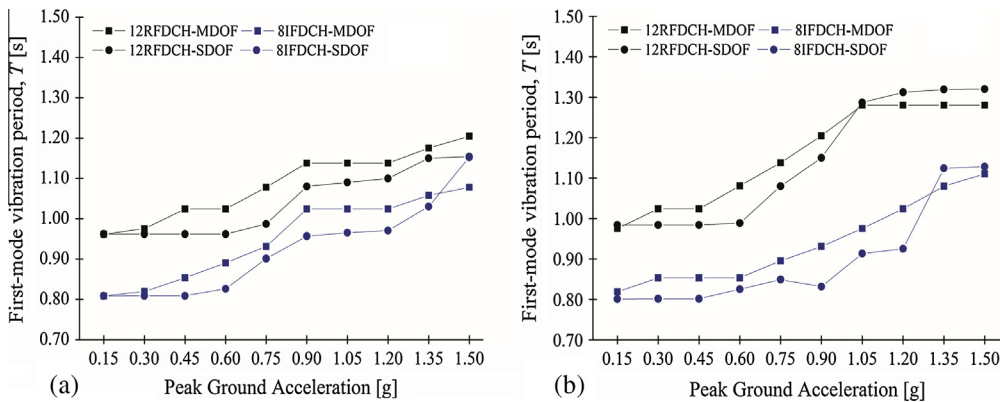


Fig. 9. Elongation of the first-mode periods with PGA, as predicted by the MDOF and the equivalent SDOF for the 12RFDCH and 8IFDCH buildings (mild degradation case), when subjected to (a) the Whittier Narrows and (b) the Hector Mine seismic motions.

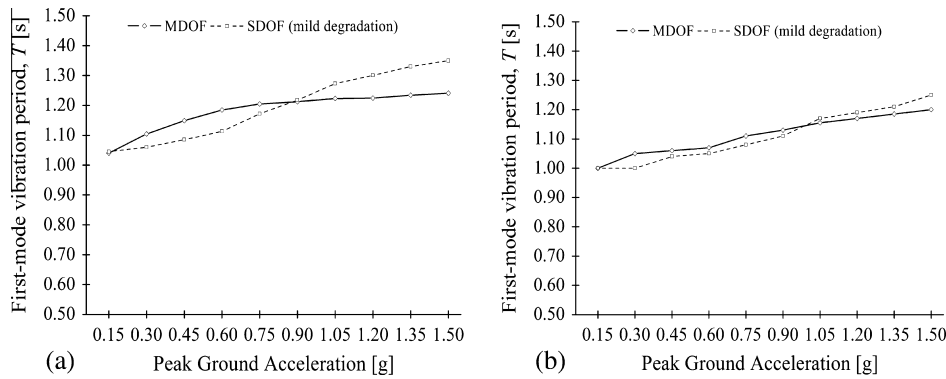


Fig. 10. Mean of the inelastic periods T_{in} predicted by the MDOF and the equivalent SDOF systems for (a) the 12RFDCH and (b) the 12RFDCL buildings using the entire subset of 20 ground motions.

motions used) for both the SDOF systems examined. More specifically, when considering the Northridge motion scaled to 0.15 g (Fig. 13a), the SDOF systems, which were modeled using either the mild or the severe degradation rule, remained fully elastic, since the predicted predominant periods were calculated equal to the elastic period of the 12RFDCH-SDOF system ($T_{el,12RFDCH-SDOF} = 0.966$ s). However, for the next intensity level considered (i.e., 0.30 g), both the mildly and the severely degrading 12RFDCH-SDOF systems responded inelastic and their predominant period estimates were calculated longer than the elastic one of the 12RFDCH-SDOF model (i.e., $T_{0.30g,milddegr.} = 0.978$ s, $T_{0.30g,sev.degr.} = 1.004$ s). In other words, the degrading rules applied to the systems do not affect their elastic response (i.e., the yield points of the models are defined irrespectively of the degradation

rule), while the mild or severe degrading models are anticipated to affect the systems response after yield limit. Once this threshold value is exceeded, the first-mode vibration period is monotonically lengthened as the ground motion becomes more intense.

5. Correlation of period elongation with intensity measures and engineering demand parameters

5.1. Parametric analysis scheme

After the above careful verification that the equivalent SDOF systems developed are accurate representations of the initial MDOF systems and reliable predictors of the inelastic period of

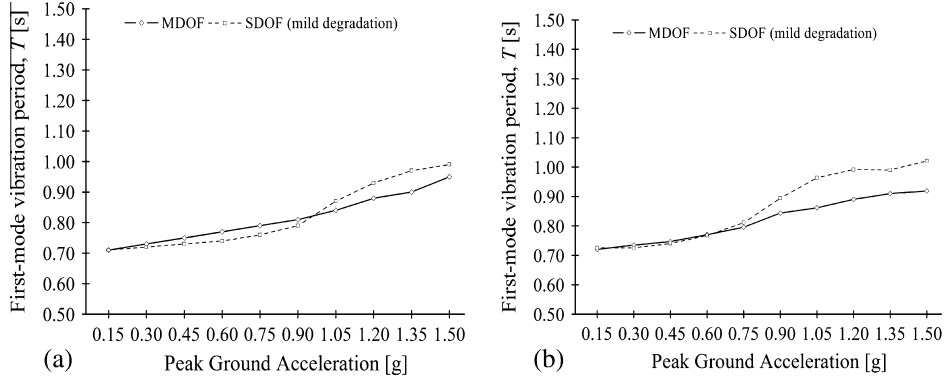


Fig. 11. Mean of the inelastic periods T_{in} predicted by the MDOF and the equivalent SDOF systems for (a) the 8SWDCH and (b) the 8SWDCL buildings using the entire subset of 20 ground motions.

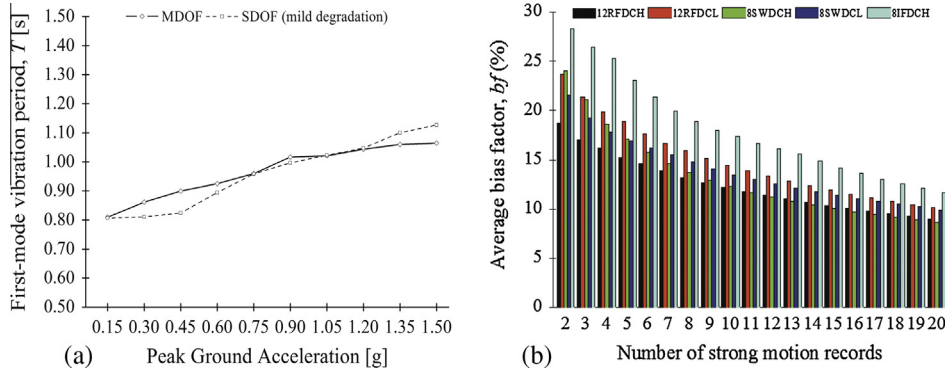


Fig. 12. (a) Mean of the inelastic periods T_{in} predicted by the MDOF and the equivalent SDOF systems for the 8IFDCH building using the subset of 20 ground motions. (b) Average bias factor of the MDOF and SDOF inelastic period estimations as a function of the number of strong ground motions used.

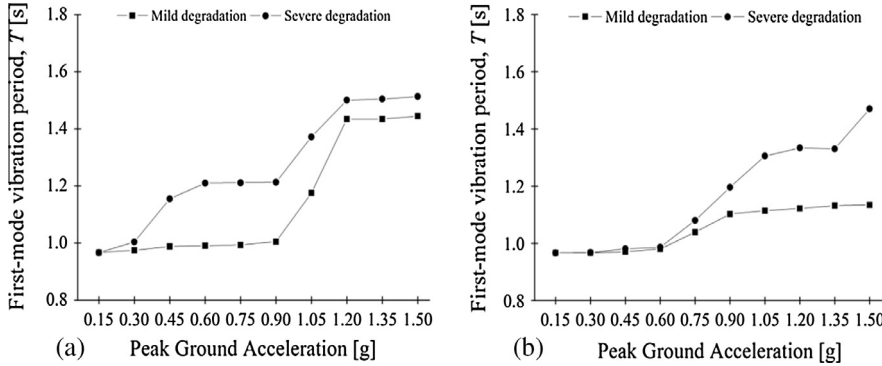


Fig. 13. Elongation of the first-mode periods with PGA for the 12RFDCH-SDOF system modeled with two degrading rules (mild and severe) after (a) the Northridge and (b) the Coyote Lake seismic motions.

the buildings studied, the equivalent models were subjected to the extended ensemble of 300 earthquake records described in Section 2. All seismic motions were scaled incrementally with scaling factors from 1 to 3.5 with a step of 0.25 (essentially up to 1.70 g) to cover variable strong motion intensity levels and various stages of seismic response starting from purely elastic behavior, initial cracking, post-yield up to severe damage. Overall, a total of 33,000, in plane, response history analyses (RHA) were performed (5 SDOF models, 2 degrading hysteretic rules, 300 seismic motions, 11 scaling factors). It is noted that for some extreme cases where the spectral acceleration at the fundamental period ($Sa(T_{el,SDOF})$) of the models exceeded 2.5 g, the response history analyses failed to converge indicating structural collapse. As expected, this was more profound for the systems modeled with the severely

degrading hysteretic rule. For this reason, an upper bound of $Sa(T_{el,SDOF})$ equal to 2.5 g was set for the parametric study, thus filtering out approximately 5% of the inelastic response results.

As previously, the predominant inelastic period, T_{in} , was derived by the Fast Fourier Transform (Fig. 8) and the period shift ratio ($T_{in}/T_{el,SDOF}$) was predicted by the elastic period ($T_{el,SDOF}$) of the equivalent SDOF systems (Section 3.2), henceforth denoted as T_{el} for simplicity. Using this extensive inelastic performance database it was made feasible to investigate the correlation of the first-mode period elongation with various intensity measures for the five structural systems studied and for various hysteretic rules adopted. The results are shown in Figs. 14–18, where the period shift ratio, T_{in}/T_{el} , is plotted for both the mildly and severely degrading systems, with: (a) the peak ground acceleration (PGA)

of the seismic motions, (b) the spectral acceleration ($S_a(T_{el})$) defined at the elastic period of each equivalent SDOF system, (c) the normalized period ratio (T_{el}/T_m) of the elastic period of the SDOF system over the mean period of the ground motion used and (d) the displacement ductility demand (μ_δ), determined as the ratio between the peak lateral inelastic displacement demand (δ_{in}) and the yield displacement (δ_y) of the systems studied:

$$\mu_\delta = \frac{\delta_{in}}{\delta_y} \quad (8)$$

In the following, the correlation between the period shift ratio, T_{in}/T_{el} , and the earlier parameters (PGA, $S_a(T_{el})$, T_{el}/T_m and μ_δ) is discussed.

5.2. Correlation of first-mode period elongation with peak ground acceleration

It is widely accepted that peak ground acceleration is only weakly correlated with the inelastic structural response independent of whether the latter is expressed in terms of drift ratio, ductility demand or energy-related damage indices [35,36]. This inefficiency of PGA is further confirmed by this study when using the predominant inelastic period as the principal engineering demand parameter (EDP). Figs. 14a–18a show that there is no significant trend between the PGA and period shift ratio, T_{in}/T_{el} , as predicted by the response history analyses (RHA) of the simplified models. For instance, several cases indicated that the first-mode vibration period was slightly elongated even for PGA values reaching 0.8 g or 1.0 g, while there were other systems showing significant period elongation ($T_{in}/T_{el} = 1.8\text{--}2.0$) for just moderate peak ground accelerations of 0.5 g. It is only after a high threshold of PGA equal to 1.0 g or 1.1 g (depending on the structural model and the degrading hysteretic rule considered), that a weak correlation was observed and the period shift ratio was indeed amplified with an increase in the PGA.

5.3. Correlation of first-mode period elongation with spectral acceleration

Contrary to the above, spectral acceleration $S_\alpha(T_{el})$, defined at the elastic, first-mode period of the equivalent SDOF systems, correlates better with the period shift ratio, T_{in}/T_{el} , for the five models studied and for both the degrading rules considered (mild and severe). The superiority of $S_\alpha(T_{el})$ for PGA in terms of the correlation with the inelastic response is also in agreement with previous studies [37], where it was found that $S_\alpha(T_{el})$, as a more structure-specific intensity measure, is more closely related to drift demands, primarily because deformation-based damage indices are often well correlated with first-mode response, even when the response is nonlinear [38]. The results of this study, further verify the superiority of $S_\alpha(T_{el})$ in predicting acceleration dependent EDPs such as the FFT-derived inelastic period studied. An additional comparison with alternative intensity measures such as the Cumulative Absolute Velocity [39] could possibly lead to improved correlations.

A closer observation of Figs. 14b–18b illustrating the correlation of T_{in}/T_{el} with $S_\alpha(T_{el})$ shows that the predominant inelastic period is not only increased with spectral acceleration, but it elongates at a different degree for various structures and degrading rules. To illustrate better this correlation, the best fit was sought using the least-squares technique: a sigmoidal-like, third order polynomial line was fitted for the three frame structural systems, 12RFDC (Fig. 14b), 12RFDC (Fig. 15b) and 8IFDCH (Fig. 16b) while a wider, half-sigmoidal curve was fitted to the data of the dual structural systems, namely, 8SWDCL (Fig. 17b) and 8SWDCH (Fig. 18b). It is seen that, under the same spectral acceleration, the period is

lengthened more extensively for the three frame structures (namely, 12RFDC, 12RFDC and 8IFDCH) as opposed to the dual systems studied.

Most importantly, the resulting first-mode period lengthening is rather moderate for all the buildings studied, even for extreme scenarios of high intensity and severe hysteretic degradation. For instance, for a spectral acceleration that corresponds to the design earthquake of a building modeled with the most critical (severe) degradation rule, located on very soft soil profile (namely, according to Eurocode 8 soil factor S equal to 1.2), at a site within the highest seismic zone in Europe (namely, Zone III in Greece, $a_g = 0.36$ g), where the spectral acceleration is approximately equal to $S_a(T_{el}) = 2.5a_gS = 2.5 \times 0.36$ g $\times 1.2 = 1.08$ g, the corresponding best-fitted period shift ratio, T_{in}/T_{el} , is found equal to 1.21, 1.18, 1.11, 1.08 and 1.05 for the 12RFDC, 12RFDC, 8IFDCH, 8SWDCL and 8SWDCH buildings, respectively. The same ratio for twice the design earthquake (namely, $S_a(T_{el}) = 2.16$ g) is 1.68, 1.66, 1.58, 1.56 and 1.32 for the five buildings studied.

Another statistical view of the entire sample of the 33,000 response history analyses, which correspond to each building and degradation rule considered, reveals that the 84th percentile of the T_{in}/T_{el} ratio for the mild degradation hysteretic rule, is equal to 1.162, 1.199, 1.168, 1.058 and 1.088 for the five buildings (12RFDC, 12RFDC, 8IFDCH, 8SWDCH and 8SWDCL respectively). Similarly, severe degradation leads to an increase of approximately 15% on average (presented in detail in Table 4). It is also interesting that the *absolute upper bound* (maximum value) did not exceed in any case the value of 1.86, 1.88, 1.92, 2.00 and 2.00, respectively, for the five buildings studied.

Overall, it can be claimed that in all cases studied, the expected (i.e., based on the best fit) period elongation of the buildings, is lower than 1.2 for the design earthquake even when considered located for the most unfavorable European site, it does not exceed 1.7 for twice the design earthquake and it is generally dropping for dual (frame-shear wall) structural systems and mild degradation rules. Thus, these results indicate a satisfactory, in general, structural performance of the structural configurations studied. The latter can be attributed to the fact that these buildings have been designed according to modern seismic code design and they have high yield strength, which further reduces their susceptibility to excessive inelastic deformations. It is herein recalled that the strength of the frame, dual and irregular buildings is on average approximately equal to 6000 kN, 7400 kN and 4600 kN, respectively [23].

5.4. Correlation of first-mode period elongation with the frequency content (T_{el}/T_m)

Another important characteristic of earthquake ground motion is its frequency content, quantified through the mean period (T_m) of Eq. (1), an indicator representing the inverse of the weighted average of the most prevalent frequencies of each record. Figs. 14c–18c show the correlation between the period shift ratio, T_{in}/T_{el} , and the normalized response over signal period ratio, T_{el}/T_m , calculated for each pair of equivalent SDOF and ground motion considered. It can be seen that the maximum period elongation is observed within the range $0.50 < T_{el}/T_m < 1.0$, that is, for systems whose elastic period T_{el} is lower than the predominant frequency of excitation and potentially gets closer to T_m after the first yield. On the contrary, structures of elastic period already greater than T_m (namely, $T_{el}/T_m > 1.25$) have higher probability to be subjected to reduced spectral acceleration after yield, hence naturally, are associated with lower (approximately half) period shift ratio T_{in}/T_{el} . It is noted that this dependence of the period elongation on the frequency content of strong motion, has also been observed for the inelastic displacement ratio C_μ ($C_\mu = \delta_{in}/\delta_{el}$) of other SDOF

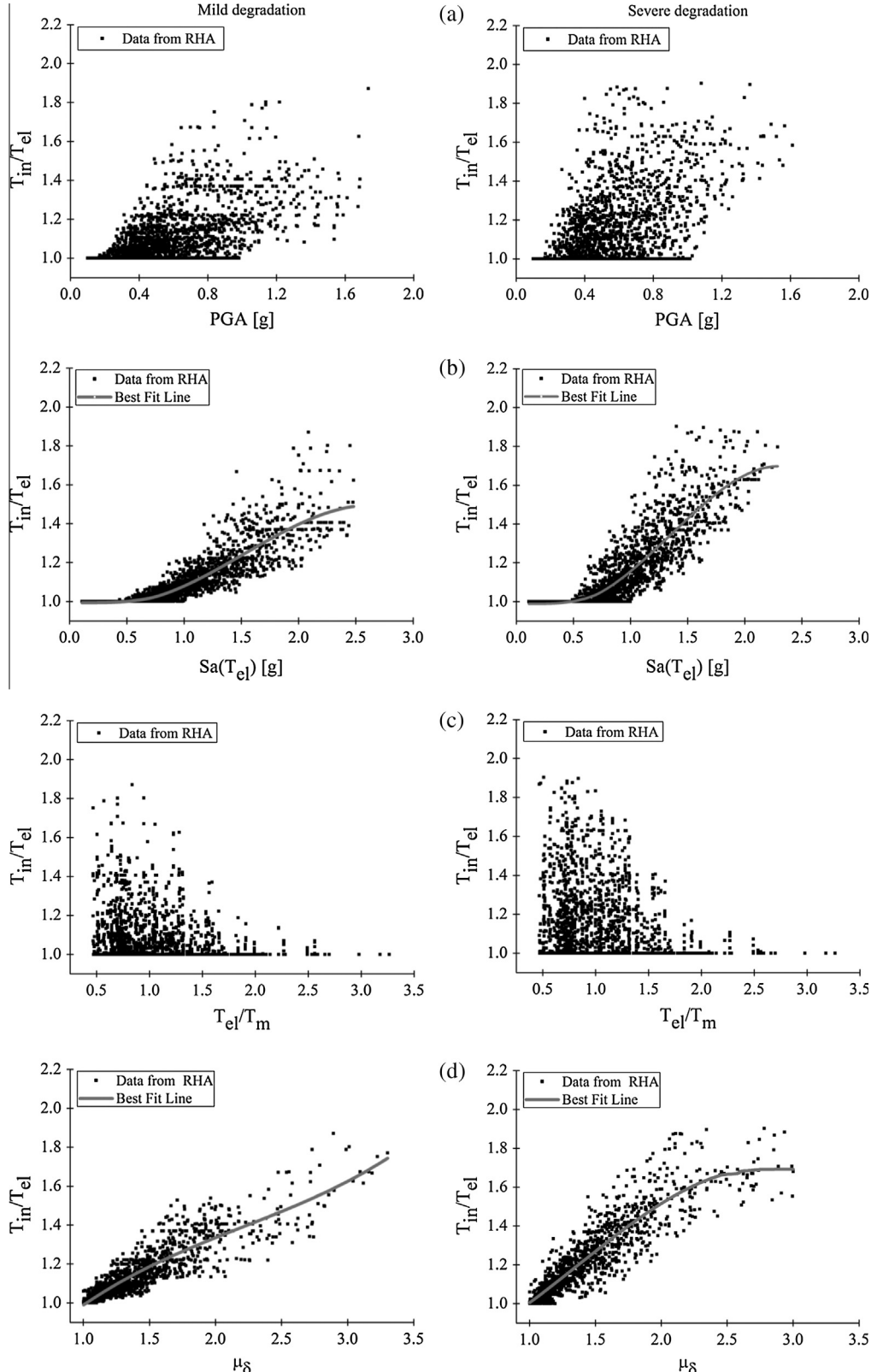


Fig. 14. Period shift ratio, T_{in}/T_{el} , versus (a) PGA, (b) $S_a(T_{el})$, (c) T_{el}/T_m and (d) μ_δ for the 12RFDCH-SDOF system modeled with two degrading hysteretic rules (mild on the left and severe on the right).

systems, such as those indicated in the literature for example [40–42].

The above sensitivity of period lengthening to the frequency content of earthquake ground motion provides further evidence that when assessing the inelastic response of structures, it is of

major importance to form sets of strong ground motions that are not only compatible with the usual, earthquake record selection criteria (i.e., magnitude, source-to-site distance), but are also unbiased in terms of the predominant frequencies of the seed records.

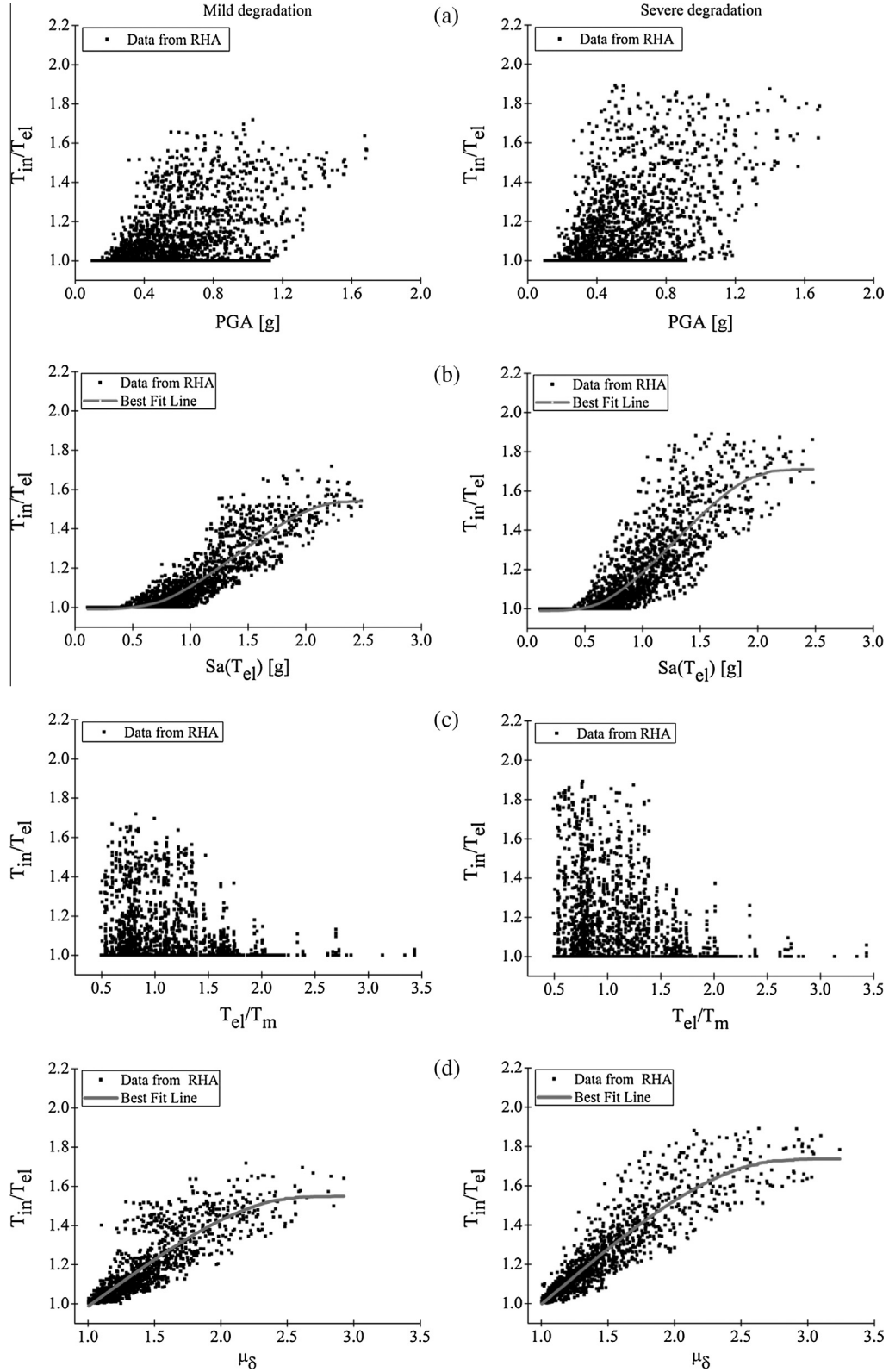


Fig. 15. Period shift ratio, T_{in}/T_{el} , versus (a) PGA, (b) $S_a(T_{el})$ (c) T_{el}/T_m and (d) μ_δ for the 12RFDCL-SDOF system modeled with two degrading hysteretic rules (mild on the left and severe on the right).

5.5. Correlation of first-mode period elongation with displacement ductility demand

Given that the period elongation is an implicit measure of structural damage, it was considered useful to investigate the

correlation between the period shift ratio, T_{in}/T_{el} , and the imposed displacement ductility demand, μ_δ . Figs. 14d–18d show a monotonic and almost linear relationship (evident especially for low-to-moderate ductility values) between T_{in}/T_{el} and the displacement ductility demand, μ_δ . It is also clear that severely degrading

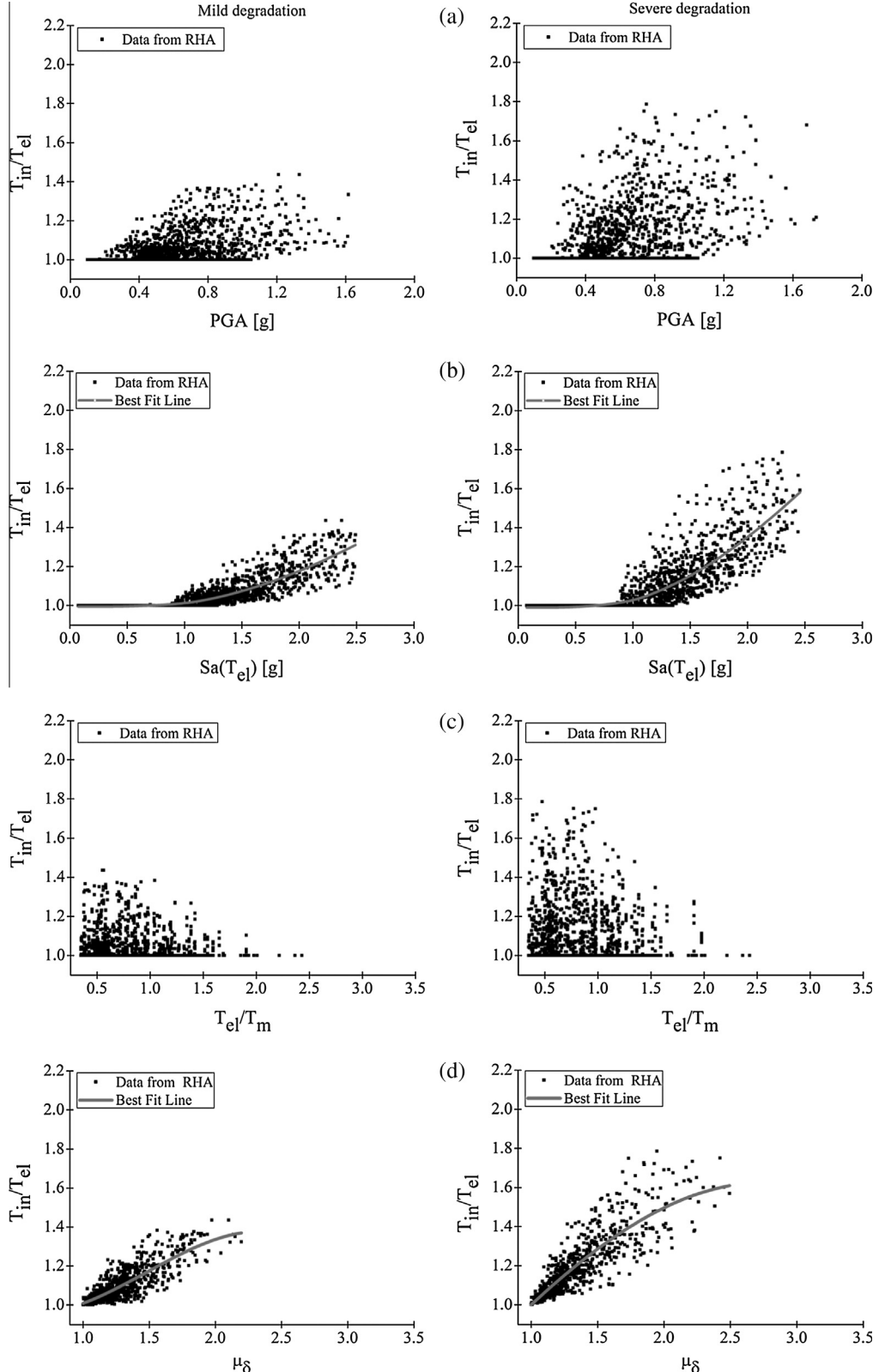


Fig. 16. Period shift ratio, T_{in}/T_{el} , versus (a) PGA, (b) $S_a(T_{el})$, (c) T_{el}/T_m and (d) μ_δ for the 8SWDCH-SDOF system modeled with two degrading hysteretic rules (mild on the left and severe on the right).

structural models (Figs. 14d–18d, right) exhibit more extensive inelastic deformations compared with the corresponding mildly degrading systems (Figs. 14d–18d, left), leading to values of μ_δ that are on average higher by 25% and to higher degrees of period elongation

(by 15–30%). This trend is in agreement with the observations made by Song and Pincheira [43], since they showed that the maximum inelastic displacements of severely degrading systems are on average higher than those of mildly degrading systems

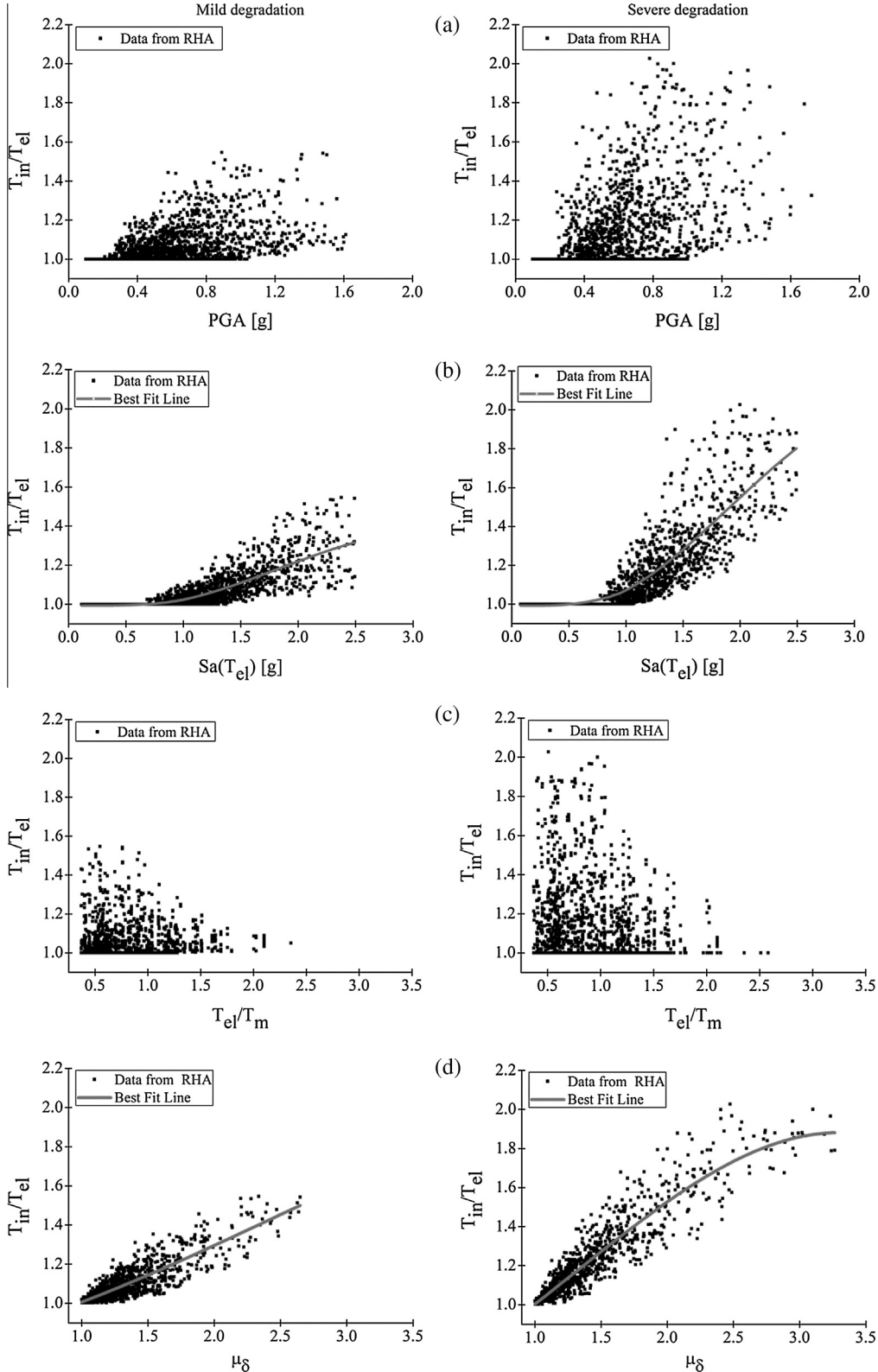


Fig. 17. Period shift ratio, T_{in}/T_{el} , versus (a) PGA, (b) $Sa(T_{el})$ (c) T_{el}/T_m and (d) μ_δ for the 8SWDCL-SDOF system modeled with two degrading hysteretic rules (mild on the left and severe on the right).

with the same initial period and strength. They also found that moderate-to-long period systems experience, on average, lower displacement amplification factors than the short period structures (namely, lower ratio of the maximum inelastic displacements using severely degrading hysteretic rules over mildly degrading

ones). This is also observed in this study (Table 5), as the two regular frame systems (12RFDC and 12RFDC), which are the most flexible of the structural systems considered, are related to the lowest displacement amplification factors, that is, they were found less sensitive on the hysteretic rule adopted.

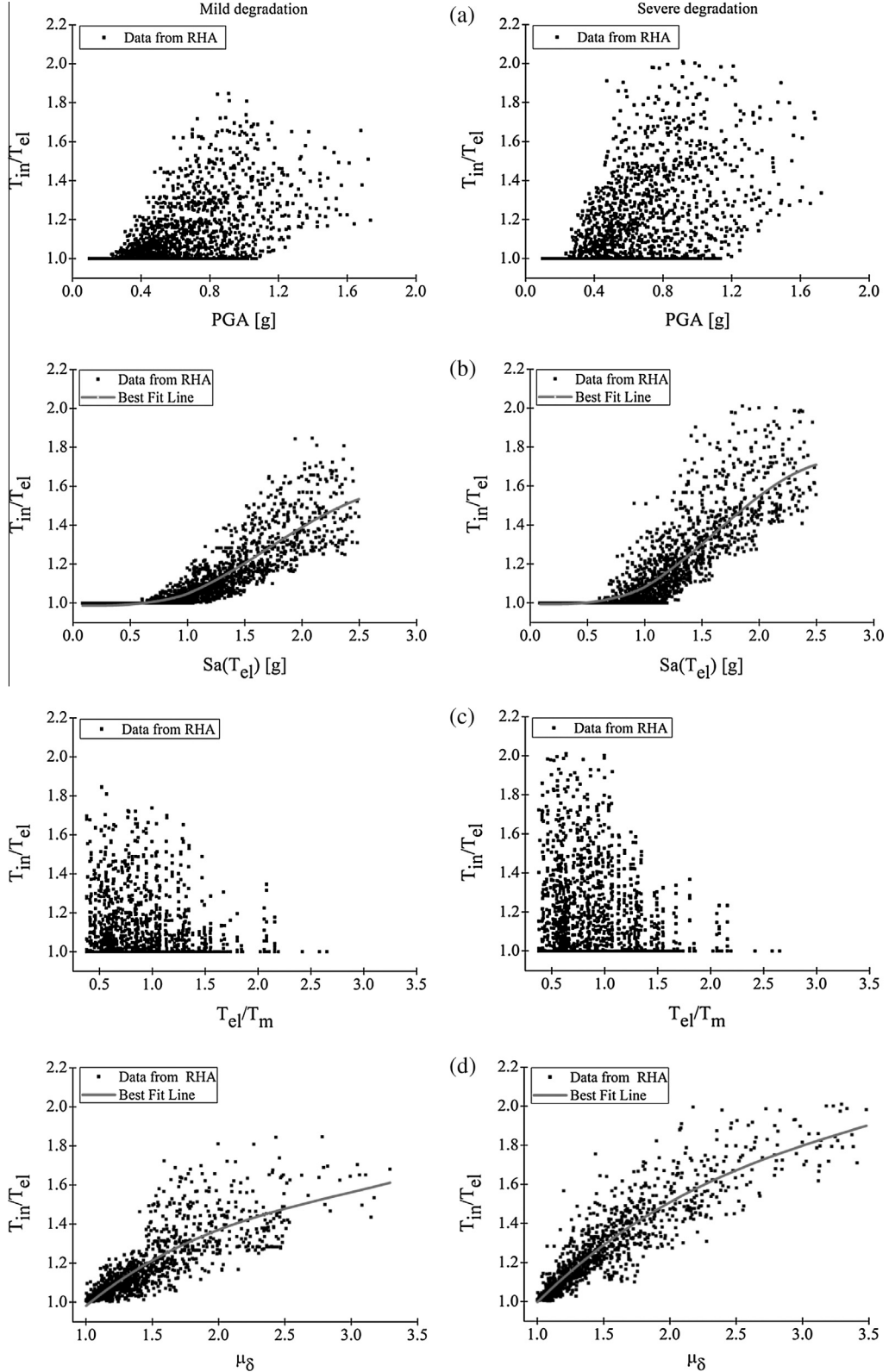


Fig. 18. Period shift ratio, T_{in}/T_{el} , versus (a) PGA, (b) $S_a(T_{el})$, (c) T_{el}/T_m and (d) μ_δ for the 8IFDCH-SDOF system modeled with two degrading hysteretic rules (mild on the left and severe on the right).

6. Implications of period elongation prediction on earthquake record selection procedures

In the light of the observations made in the previous section about the extent of first-mode period elongation of the five

buildings studied, it is of particular interest to revisit the period range imposed for spectral matching and ground motion selection purposes in most modern seismic codes (i.e., Eurocode 8, ASCE-SEI 7-10, FEMA P-750). The reason is that the bandwidth, within which the average spectrum of the records selected needs to match the

Table 4

84th and 95th percentiles of the period shift ratio estimates (16% and 5% probability of exceedance).

Structural systems	Period shift ratio (T_{in}/T_{el})		95th Percentile	
	84th Percentile		Mild degradation	Severe degradation
	Mild degradation	Severe degradation		
12RFDCH	1.162	1.298	1.366	1.508
12RFDCL	1.199	1.368	1.439	1.586
8SWDCH	1.058	1.221	1.181	1.338
8SWDCL	1.088	1.268	1.224	1.483
8IFDCH	1.168	1.325	1.396	1.555

Table 5

Displacement amplification factors derived for the severely and the mildly degrading systems.

Displacement amplification factor ($\delta_{max,in.}^{sev.deg.} / \delta_{max,in.}^{milddegr.}$) (%)					
Structural systems	12RFDCH ($T_{el} = 0.966$ s)	12RFDCL ($T_{el} = 1.038$ s)	8SWDCH ($T_{el} = 0.707$ s)	8SWDCL ($T_{el} = 0.723$ s)	8IFDCH ($T_{el} = 0.804$ s)
84th Percentile	3.56	8.07	10.90	14.50	8.63
95th Percentile	2.25	11.03	12.40	23.65	18.81

target code spectrum, depends solely on the first-mode period, T_1 , of the building in the horizontal direction of interest. This specific structural characteristic essentially controls the extent of spectral matching as the period range of interest extends from $0.2T_1$ to account for higher mode response, up to $1.5T_1$ (in ASCE-SEI 7-10, Section 16.2; FEMA P-750, Section C16.1.3.1; Eurocode 8-Part 2, Section 3.2.2.4(3)) or $2.0T_1$ (in Eurocode 8-Part 1, Section 3.2.3.1.2(4)) to account for period lengthening associated with inelastic response. It is also interesting to add that, to the best of the knowledge of the authors, both the lower (i.e., $0.2T_1$) and the upper bound of the spectral matching period range (i.e., $1.5T_1$ or $2.0T_1$) have been only qualitatively assigned.

Given that the five structures studied were designed according to modern seismic codes (herein to EC8) the observation made above that the (best fitted) period elongation of the buildings, is lower than 1.2 for the design earthquake and it does not exceed 1.7 for twice the design earthquake, is thought provoking. Particularly from the results summarized in Table 4, it is seen, as a rather extreme case, that even the 95th percentile of the T_{in}/T_{el} ratio does not exceed 1.58 irrespectively of the structural system, the hysteretic rule and the ductility class adopted. It is also noted that, especially for dual, frame-wall buildings (8SWDCL and 8SWDCH), the 95th percentile of the T_{in}/T_{el} ratio does not exceed 1.48 even in the most unfavorable combination of severe degradation and seismic hazard. This is an indication that the upper bound of the period range prescribed in the US codes ($1.5T_1$) seems to be more realistic compared to the one prescribed in Eurocode 8 ($2.0T_1$) at least for dual buildings which are characterized by high strength.

Two sources of uncertainty need to be discussed here. One is the complex behavior of such R/C structural walls entering far into the inelastic range, as well as the complex interaction of all structural elements in buildings with structural walls, which is still not adequately understood [44], thus naturally, introducing significant epistemic uncertainty in their modeling as both MDOF and SDOF systems. Secondly, Eurocode 8 does not explicitly state whether T_1 is to be taken by the designer as the first-mode vibration period ($T_{cr} \approx T_{eff,MDOF}$) assuming 50% (cracked) stiffness properties uniformly for all structural members (as prescribed for analysis but not clarified for ground motion selection) or it simply refers to the elastic first-mode period, T_{el} , as for instance is clearly the case in ASCE-SEI 7-10.

Notwithstanding the above uncertainties, it is suggested that, as long as ground motion selection relies on spectral matching and not on more refined procedures, such as the concepts of the

“Conditional Mean Spectrum” [45], the “Structure-specific Earthquake Records Selection” [46] or others (reviewed in Ref. [47]), special effort is required to define more reliably the code-imposed, spectral matching period range accounting for crucial characteristics of various types of structures. Moreover, in the case of Eurocode 8 framework of ground motion selection, it is important to relate the spectral matching range with an explicit definition of the fundamental period. Both the above issues have significant design and assessment implications as it has been shown [22,48] that an excessive spectral matching period range, often leads to unrealistically high-energy content of the seed time histories at periods close or lower to the fundamental period of the building, thus resulting to unnecessary overdesign.

7. Conclusions

The study aims to quantify the correlation between the predominant period elongation of buildings designed according to modern seismic codes and various strong-motion and demand parameters. An extensive validation procedure was performed to verify the transformation of the MDOF systems into equivalent nonlinear SDOF ones using hysteretic rules that consider the stiffness degradation, strength deterioration and pinching of the R/C members. The SDOF systems were subjected to a carefully selected set of 300 earthquake strong motions and the predominant inelastic period was identified using the Fast Fourier Transformation algorithm. The principal conclusions drawn from this study can be summarized as follows:

- (1) No significant dependence was observed between the predominant inelastic period and the peak ground acceleration, corroborating the minor correlation of PGA with the inelastic structural response parameters. On the contrary, spectral acceleration was found more closely related to the inelastic response.
- (2) The predicted period elongation for all the five buildings was found lower than 1.2 for the design earthquake, even when considering the more earthquake prone European site. The predicted T_{in}/T_{el} ratio did not also exceed 1.7 for twice the design earthquake, while it was lower for dual (frame-shear wall) or mildly degrading structural systems.
- (3) It is considered necessary to revisit the period range prescribed in Eurocode 8 for spectral matching of earthquake records, especially for dual systems, whose 95th percentile

- of T_{in}/T_{el} ratio was found lower than 1.5. On the contrary, the period range prescribed in the US codes (ASCE-SEI 7-10, FEMA P-750), extending up to 1.5 times the fundamental period, seems to agree better with the observations made.
- (4) The first-mode period elongation is correlated with the frequency content of seismic excitation. Systems with elastic period lower than the predominant period of excitation ($0.50 < T_{el}/T_m < 1.0$) lead to T_{in}/T_{el} ratio being almost double than that observed in systems with $T_{el}/T_m > 1.25$. A monotonic and relatively linear relationship was also observed between the elongated period and the displacement ductility demand (μ_d). The severely degrading systems exhibited higher μ_d (by 25%) and T_{in}/T_{el} ratio (by 15–30%).

The results presented herein are dependent on both the specific types of buildings considered (i.e., structures designed according to contemporary seismic codes) and the assumptions adopted to predict the inelastic periods (i.e., MDOF-to-SDOF transformation). Further research is needed both to quantify thoroughly the first-mode period elongation of structures and to justify the breadth of the code-imposed, spectral matching period window especially tailoring the particular characteristics of different types of structures.

Acknowledgement

This research was partially supported by the 7th Frame-work Programme of the European Commission, under the PIRSES-GA-2009-247567-EXCHANGE-SSI (Experimental & Computational Hybrid Assessment Network for Ground-Motion Excited Soil-Structure Interaction Systems) Grant. This support is gratefully appreciated.

References

- [1] Udwadia FE, Trifunac DM. Time and amplitude dependent response of structures. *Earthquake Eng Struct Dyn* 1974;2:359–78.
- [2] Roufael MSL, Meyer C. Analytical modeling of hysteretic behavior of r/c frames. *J Struct Eng* 1987;113:429–44.
- [3] Dipasquale E, Ju J-W, Askar A, Cakmak AS. Relation between global damage indices and local stiffness degradation. *J Struct Eng* 1990;116:1440–56.
- [4] Williams MS, Sexsmith RG. Seismic damage indices for concrete structures: a state-of-the-art review. *Earthquake Spectra* 1995;11:319–49.
- [5] Massumi A, Moshtagh E. A new damage index for RC buildings based on variations of nonlinear fundamental period. *Struct Des Tall Special Build* 2013;22(1):50–61.
- [6] Kadas K, Yakut A, Kazaz I. Spectral ground motion intensity based on capacity and period elongation. *J Struct Eng* 2011;137:401–9.
- [7] Trifunac DM, Ivanovic SS, Todorovska IM. Apparent periods of a building. II: Time-frequency analysis. *J Struct Eng* 2001;127:527–37.
- [8] Mucciarelli M, Masi A, Gallipoli MR, Harabaglia P, Vona M, Ponzo F, et al. Analysis of RC building dynamic response and soil-building resonance based on data recorded during a damaging earthquake (Molise, Italy, 2002). *Bull Seismol Soc Am* 2004;94:1943–53.
- [9] Clinton JF, Bradford CS, Heaton TH, Favela J. The observed wander of the natural frequencies in a structure. *Bull Seismol Soc Am* 2006;96:237–57.
- [10] Kashima T, Kitagawa Y. Dynamic characteristics of buildings estimated from strong motion records. In: 8th National conference on earthquake engineering, San Francisco, US; 2006.
- [11] Masi A, Vona M. Experimental and numerical evaluation of the fundamental period of undamaged and damaged RC framed buildings. *Bull Earthquake Eng* 2010;8:643–56.
- [12] Pinho R, ElNashai AS. Dynamic collapse testing of a full-scale four storey RC frame. *ISET J Earthquake Technol* 2000;37:143–63.
- [13] Pegon P, Pinto AV. Pseudo-dynamic testing with substructuring at the ELSA laboratory. *Earthquake Eng Struct Dyn* 2000;29:905–25.
- [14] Jeong S-H, ElNashai AS. Analytical assessment of an irregular RC full scale 3D test structure. Department of Civil and Environmental Engineering, University of Illinois at Urbana-Champaign, Urbana, Illinois; 2004.
- [15] Zembaty Z, Kowalski M, Pospisil S. Dynamic identification of a reinforced concrete frame in progressive states of damage. *Eng Struct* 2006;28:668–81.
- [16] Calvi GM, Pinho R, Crowley H. State-of-the-knowledge on the period elongation of RC buildings during strong ground shaking. In: 1st European conference of earthquake engineering and seismology, Geneva, Switzerland; 2006.
- [17] Dunand F, Gueguen P, Bard P-Y, Rodgers J, Celebi M. Comparison of the dynamic parameters extracted from weak, moderate and strong motion recorded in buildings. In: 1st European conference of earthquake engineering and seismology, Geneva, Switzerland; 2006.
- [18] Michel C, Gu P, Arem SE, Mazars J, Kotronis P, Guéguen P. Full-scale dynamic response of an RC building under weak seismic motions using earthquake recordings, ambient vibrations and modelling. *Earthquake Eng Struct Dyn* 2010;39:419–41.
- [19] CEN. European Standard EN 1998-1. Eurocode 8: Design of structures for earthquake resistance. Part 1: General rules, seismic actions and rules for buildings. Comité Européen de Normalisation, Brussels. Brussels, Belgium: European Committee for Standardization; 2004.
- [20] ASCE. Minimum design loads for buildings and other structures. ASCE Standard No. 7-10. Reston, VA; 2010.
- [21] FEMA P-750. NEHRP Recommended seismic provisions for new buildings and other structures. Washington, DC; 2009.
- [22] Sextos AG, Katsanos EI, Manolis GD. EC8-based earthquake record selection procedure evaluation: validation study based on observed damage of an irregular R/C building. *Soil Dyn Earthquake Eng* 2011;31:583–97.
- [23] Papanikolaou VK, ElNashai AS. Evaluation of conventional and adaptive pushover analysis. I: methodology. *J Earthquake Eng* 2005;9:923–41.
- [24] Fajfar P. A nonlinear analysis method for performance-based seismic design. *Earthquake Spectra* 2000;16:573–92.
- [25] Rathje EM, Faraj F, Russell S, Bray JD. Empirical relationships for frequency content parameters of earthquake ground motions. *Earthquake Spectra* 2004;20:119–44.
- [26] Chiou B, Darragh R, Gregor N, Silva W. NGA Project strong-motion database. *Earthquake Spectra* 2008;24:23–44.
- [27] Fardis MN. Analysis and design of reinforced concrete buildings according to Eurocodes 2 and 8, Configurations 3, 5 and 6. Reports on Prenormative Research in Support of Eurocode 8; 1994.
- [28] Mwafy AM, ElNashai AS. Static pushover versus dynamic collapse analysis of RC buildings. *Eng Struct* 2001;23:407–24.
- [29] ElNashai AS, Papanikolaou VK, Lee D, Zeus NL. A system for inelastic analysis of structures. Univ. of Illinois at Urbana-Champaign; 2002.
- [30] Fajfar P, Gasparic P. The N2 method for the seismic damage analysis of RC buildings. *Earthquake Eng Struct Dyn* 1996;25:31–46.
- [31] Reinhorn AM, Roh H, Sivaselvan M, Kunath SK, Valles RE, Madan A, et al. IDARC2D Version 7.0: a program for the inelastic damage analysis of structures. University at Buffalo, State University of New York; 2009.
- [32] Park Y-J, Ang AH, Wen YK. Damage-limiting aseismic design of buildings. *Earthquake Spectra* 1987;3:1–26.
- [33] Vamvatsikos D, Cornell CA. Incremental dynamic analysis. *Earthquake Eng Struct Dyn* 2002;31:491–514.
- [34] Lin L, Naumoski N, Foo S, Saatcioglu M. Elongation of the fundamental periods of reinforced concrete frame buildings during nonlinear seismic response. In: 14th World conference on earthquake engineering, Beijing, China; 2008.
- [35] Kurama YC, Farrow KT. Ground motion scaling methods for different site conditions and structure characteristics. *Earthquake Eng Struct Dyn* 2003;32:2425–50.
- [36] Giovenale P, Cornell CA, Esteve L. Comparing the adequacy of alternative ground motion intensity measures for the estimation of structural responses. *Earthquake Eng Struct Dyn* 2004;33:951–79.
- [37] Shome N, Cornell CA, Bazzurro P, Carballo EJ. Earthquakes, records and nonlinear responses. *Earthquake Spectra* 1998;14:469–500.
- [38] Haselton CB, Baker JW, Liel AB, Deierlein GG. Accounting for ground motion spectral shape characteristics in structural collapse assessment through an adjustment for epsilon. *J Struct Eng* 2009;332–44.
- [39] Campbell KW, Bozorgnia Y. A ground motion prediction equation for the horizontal component of cumulative absolute velocity (CAV) based on the PEER-NGA strong motion database. *Earthquake Spectra* 2010;26:635–50.
- [40] Chopra AK, Chintanapakdee C. Inelastic deformation ratios for design and evaluation of structures: single-degree-of-freedom bilinear systems. *J Struct Eng* 2004;130:1309–19.
- [41] Kumar M, Castro JM, Stafford PJ, Elghazouli AY. Influence of the mean period of ground motion on the inelastic dynamic response of single and multi degree of freedom systems. *Earthquake Eng Struct Dyn* 2011;40:237–56.
- [42] Ruiz-García J, Miranda E. Inelastic displacement ratios for evaluation of structures built on soft soil sites. *Earthquake Eng Struct Dyn* 2006;35:679–94.
- [43] Song J-K, Pincheira J-A. Spectral displacement demands of stiffness-and-strength-degrading systems. *Earthquake Spectra* 2000;16:817–51.
- [44] Fischinger M, Rejec K, Isakovic T. Seismic behavior of RC structural walls and Eurocode 8 provisions. In: 9th US National and 10th Canadian conference on earthquake engineering, Toronto, Canada; 2010.
- [45] Baker J. Conditional mean spectrum: tool for ground motion selection. *J Struct Eng* 2011;137:322–31.
- [46] Katsanos EI, Sextos AG. ISSARS: an integrated software environment for structure-specific earthquake ground motion selection. *Adv Eng Software* 2013;58:70–85.
- [47] Katsanos EI, Sextos AG, Manolis GD. Selection of earthquake ground motion records: a state-of-the-art review from a structural engineering perspective. *Soil Dyn Earthquake Eng* 2010;30:157–69.
- [48] Lew M, Naeim F, Hudson M, Korin B. Challenges in specifying ground motions for design of tall buildings in high seismic regions of the United States. In: 14th world conference on earthquake engineering, Beijing, China; 2008.